Multidisciplinary Journal of Engineering and Technology
Print ISSN: 3007-6897
Online ISSN: 3007-6900
DOI: https://doi.org/10.61784/mjet3040

STABILITY ANALYSIS OF OPEN-PIT SLOPES IN COLD REGIONS BASED ON REDUCTION OF ROCK MASS MECHANICAL PARAMETERS

ZhaoLong Diao[1], Dong Lu[1*], YongQuan Liu[2], GuoDong Li[2], ZhiQuan Xu[2]
[1]Xinjiang Jinchuan Mining Co., Ltd., Yining 835000, Xinjiang, China.
[2]Shandong Gold Jinchuang Group Co., Ltd., Yantai 264000, Shandong, China.
[*]Corresponding Author: Dong Lu

Abstract: Open-pit slopes in alpine mining areas of western China are significantly affected by freeze-thaw cycles, snowmelt infiltration and weathering, leading to severe deterioration of rock mechanical properties and difficulties in stability evaluation. Taking the rock slopes of Jingxi-Barak open-pit mining area of Xinjiang Jinchuan Mining Co., Ltd. as the research object, laboratory rock mechanical tests, rock mass strength parameter reduction and numerical stability analysis of slopes were carried out. Field sampling, standard specimen preparation and indoor mechanical tests were performed to systematically obtain physical and mechanical parameters including compressive strength, tensile strength and shear strength of four types of rock masses (tuff, limestone, tuffaceous sandstone and crystal tuff) under natural and saturated conditions. Combined with the structural characteristics of rock mass and excavation disturbance in the mining area, reasonable reduction of mechanical parameters of in-situ rock mass was realized. Numerical models of typical slope profiles were constructed, and seepage field analysis was conducted via the Seep/W module. The Sarma method and Spencer method were adopted to implement limit equilibrium stability calculations. The results show that the safety factors of slopes in the study area range from 2.077 to 2.247, which are higher than the allowable safety factor of 1.25 specified in relevant codes, indicating the overall good stability of slopes in the mining area. The research results can provide experimental basis and technical reference for slope safety evaluation, excavation design and geological disaster prevention and control of open-pit mines in cold alpine regions.
Keywords: Open-pit mine; Slope stability; Parameter reduction; Load combination

1 INTRODUCTION

With the growth of domestic economy, the demand for mineral resources has increased continuously, while mineral reserves in eastern China are gradually depleted. Abundant mineral resources are distributed in cold alpine regions of western China, and the stability of open-pit slopes in such regions is the key factor restricting safe and efficient mineral exploitation.

In terms of rock slope research, Zheng Yingren et al. made vital breakthroughs based on the limit equilibrium method for multi-step slopes[1], and innovatively established a limit equilibrium analysis system for multi-stage composite slopes. Gu Dezhen, Sun Yuke et al. adopted stereographic projection to analyze the stability of rock slopes[2-4]. Fan Gang et al. carried out slope model tests and shaking table tests to study the stability of various slopes[5], and the results revealed that anti-dip slopes possess remarkably higher stability than bedding slopes. Goodman & Kieffer classified six deformation and failure modes of rock slopes according to the combination relationship between joint planes and slope surfaces[6]. Li Ze et al. proposed a lower bound finite element limit analysis method for rock slopes considering nonlinear mechanical characteristics[7]. Zuo Baocheng et al. developed an independent three-dimensional geomechanical simulation system and revealed the instability evolution mechanism of anti-dip rock mass structures[8]. Ding Xiuli et al. established a graded loading creep test system for rock mass with lithological differences[9], and systematically clarified the time-dependent deformation mechanism of layered composite rock masses. Guo Zhu et al. constructed a numerical model for seismic dynamic response and illustrated the multi-field coupling evolution law of rock slopes under seismic loads[10]. Huang Qiuxiang et al. conducted in-depth research on the failure mechanism of anti-dip layered rock slopes[11].

In summary, according to the above domestic and international research progress, abundant achievements have been obtained regarding the stability of rock slopes in eastern China. Nevertheless, studies focusing on open-pit slope stability under special cold-region environments remain insufficient, and few investigations integrate rock mass mechanical parameter reduction into slope stability evaluation.

2 LABORATORY PHYSICAL AND MECHANICAL TESTS OF ROCK SPECIMENS

Rock mass is a complex medium cut by numerous discontinuous structural planes formed by long-term tectonic movements, exhibiting complicated engineering mechanical properties that cannot be fully characterized by current research techniques. For a long time, the determination of rock mass strength parameters has been a tough problem troubling the engineering community. Comprehensive experimental methods are required to determine the shear strength of rock masses for slope stability research, which has attracted extensive attention from engineering practitioners.

2.1 Field Sampling and Specimen Preparation

Based on geological data and borehole records of Xinjiang Jinchuan Mining Co., Ltd., relatively intact rock blocks meeting test and processing requirements were collected from existing geological exploration sites. A total of 48 intact rock blocks of four types of structural rock masses from the Jingxi-Barak mining area were obtained. The field sampling scenes of different rock types are shown in Figure 1.

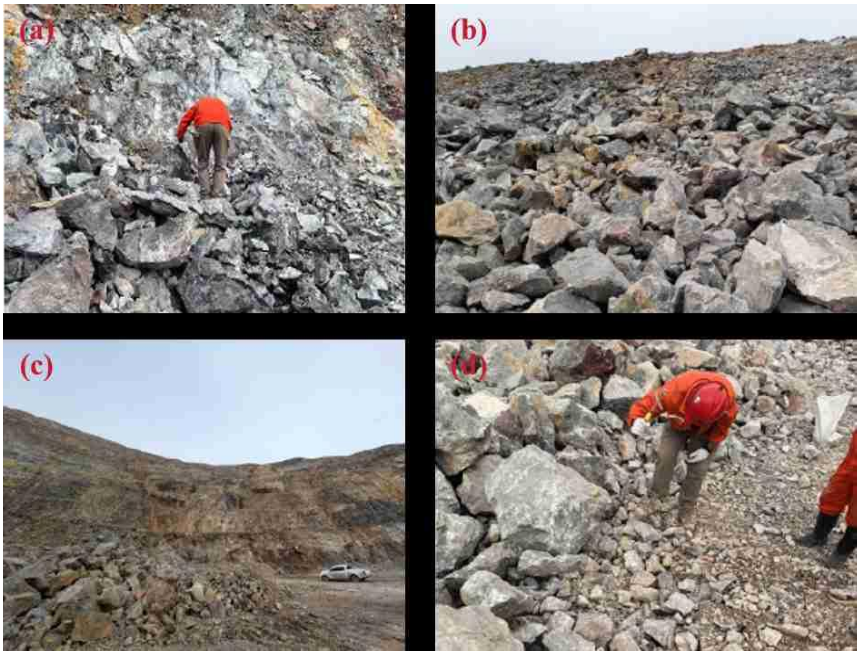

Figure 1 Field Sampling Photos of Different Rock Types: (a) Tuff; (b) Limestone; (c) Tuffaceous Sandstone; (d) Crystal Tuff

Standard machined specimens are presented in Figure 2.

Figure 2 Machined Standard Test Specimens: (a) Standard Uniaxial Compression Specimen; (b) Standard Brazilian Disc Specimen; (c) Standard Variable-Angle Shear Specimen

Saturated specimens were treated with a ZK-2700 vacuum saturation cylinder complying with the specimen preparation and saturation specifications specified in GB/T 50123-1999 Standard for Geotechnical Test Methods. The vacuum saturation procedure was performed as follows: maintain a vacuum pressure of −0.08 ~ −0.095 MPa for no less than 2 h, followed by immersion in atmospheric pressure pure water for 24 h. Before vacuum pumping, sufficient pure water was injected into the cylinder to fully submerge all specimens. The vacuum pump was then activated to reduce the internal pressure below −0.1 MPa, and the valve and pump were closed for pressure holding until full saturation was achieved. Natural-state specimens were merely cleaned and placed in a constant temperature and humidity environment (20±2 ℃, relative humidity 50%-70%) for standing treatment.

2.2 Test Methods and Principles

The deformation and failure characteristics of rock under different stress states are described by physical and mechanical parameters acquired via laboratory tests, including compression tests, tensile tests and triaxial tests. Key parameters involve elastic modulus, Poisson’s ratio, uniaxial compressive strength, cohesion and internal friction angle, which serve as essential input data for constitutive models (e.g., Mohr-Coulomb model and Drucker-Prager model) in numerical simulations. Parameters measured from laboratory tests can make numerical simulations reproduce the actual mechanical behaviors of rock masses accurately. Therefore, indoor physical and mechanical tests provide fundamental data and verification criteria for numerical modeling, ensuring reliable simulation results that match practical engineering conditions.

Uniaxial compression tests and Brazilian splitting tensile tests were adopted to measure rock compressive and tensile strength respectively, following the testing standards recommended by the International Society for Rock Mechanics (ISRM). Specimens for uniaxial compression tests adopt a height-diameter ratio of 2–2.5 with dimensions of Φ50 mm×100 mm; disc specimens for Brazilian splitting tests have a thickness-diameter ratio of 0.5-1.0 with dimensions of Φ50 mm×25 mm. Both ends of all specimens were ground and polished to guarantee flatness less than 0.05 mm and parallelism less than 0.02 mm.

Variable-angle shear tests were conducted on cubic specimens with dimensions of 30 mm×30 mm×30 mm and dimensional error controlled within 0.2-0.3 mm. All surfaces were strictly parallel with parallelism deviation less than 0.07 mm and surface protrusion less than 0.03 mm. Three shear angles were set for each rock type, and three replicate specimens were tested at each angle, with average values adopted as final test results.

All tests were carried out on an EHC-3100 microcomputer-controlled electro-hydraulic servo universal testing machine. The relative indication error of test force is less than ±1% of the actual value. The testing machine adopts a seamless heavy-duty frame with high rigidity and tiny deformation, which ensures small errors in repeated tests. Excellent centering and coaxiality minimize lateral force on loaded specimens, satisfying the coaxiality detection methods specified in GB/T 16491-1996 Electronic Universal Testing Machines and ASTM E1012-5.

2.3 Rock Mechanical Parameters

A summary of physical and mechanical properties of rock specimens is listed in Table S1.

3 ROCK MASS STRENGTH REDUCTION BASED ON THE HOEK-BROWN CRITERION

The Geological Strength Index (GSI) system is a widely accepted method for determining rock mass mechanical parameters and has been integrated into programming tools. It evaluates rock mass quality through field geological surveys and calculates rock mass strength by combining the Hoek-Brown failure criterion. The core principle of GSI evaluation lies in the characterization of two fundamental parameters: intact rock uniaxial compressive strength and the material constant related to rock frictional properties. Hoek proposed an empirical formula correlating GSI and Barton’s rock mass quality index Q based on extensive engineering case comparisons:

$$GSI = 9\ lnQ + 44 \tag{1}$$

where Q = Barton rock mass quality index.

In this study, Barton Q classification, GSI rock mass evaluation and laboratory rock mechanical test data were integrated to calculate rock mass mechanical parameters via the Hoek-Brown criterion. The calculation procedures are as follows: calculate GSI values from field-measured Q values, then substitute GSI and intact rock laboratory parameters into the Hoek-Brown criterion to obtain equivalent mechanical parameters of fractured rock masses.

The Hoek-Brown criterion has been revised and extended through decades of applications in slope engineering, tunnels and mining projects, incorporating geological conditions of rock masses (rock mass structure, joint surface roughness, etc.) via the GSI index. In 2018, Hoek and Brown published The Hoek-Brown failure criterion and GSI-2018 edition in the Journal of Rock Mechanics and Geotechnical Engineering sponsored by the Chinese Society for Rock Mechanics and Engineering, marking the formation of a nearly finalized version of this empirical criterion. Compared with the 1995 edition, the 2018 version introduces a quantitative disturbance factor D ranging from 0 to 1, covering both underground and surface rock engineering. For surface engineering, it includes open-pit mines and building slopes; for underground engineering, it distinguishes blasting excavation and tunnel boring machine excavation.

The nonlinear strength relationship of rock masses defined by the updated 2018 Hoek-Brown criterion describes the correlation between major and minor principal stresses at failure for intact rock and fractured rock masses:

$$\sigma_1 = \sigma_3 + \sigma_c\left(m_b\frac{\sigma_3}{\sigma_c} + s\right)^{\alpha} \tag{2}$$

where:

σ_1 —major principal stress at failure, MPa;

σ_3 —minor principal stress applied on rock specimens, MPa;

σ_c —uniaxial compressive strength of intact rock, MPa;

mb, s, a —semi-empirical parameters reflecting rock mass characteristics.

$$m_b = m_i exp\left(\frac{GSI-100}{28-14D}\right) \tag{3}$$

Where：

m_i —Hoek-Brown constant of intact rock.

In Equation (2), the minimum principal stress is specified σ_3 =0， The compressive strength of engineering rock mass σ_{cm} can be determined from laboratory strength tests of rock specimens.

$$\sigma_{cm}=\sigma_c s^a \tag{4}$$

Where：

σ_{cm} —overall strength of jointed rock mass，MPa

For intact rock， s=1， $\sigma_{cm}=\sigma_c$ ， this refers to the compressive strength of intact rock blocks; while for fractured rock,s<1。

Furthermore, by substituting $\sigma_1=\sigma_2=\sigma_{tm}$ into Equation (2) which represents the biaxial tensile condition, the uniaxial tensile strength σ_{tm} of rock mass is expressed as follows:

$$\sigma_{tm}=0.5\sigma_c\left(m_b-\sqrt{m_b^2+4\mathrm{s}}\right) \tag{5}$$

4 SLOPE STABILITY ANALYSIS

4.1 Selection of Calculation Profiles

According to the mining site layout, slope stability zoning, geological structural characteristics and potential failure modes of open-pit slopes in Xinjiang Jinchuan Mining Area, 15 typical cross-sections were selected for limit equilibrium analysis. These profiles comprehensively cover major slope orientations and potential slip zones of the Jingxi-Barak mining area, Kuanggou mining area and the eastern slope of the concentrator plant. The distribution of slope zones and typical profiles is shown in Figure 3.

Figure 3 Zoning Map of Open-Pit Slopes and Layout of Typical Calculation Profiles
(Source: Xinjiang Jinchuan Mining Co., Ltd)

4.2 Establishment of Numerical Calculation Models

Two-dimensional limit equilibrium analysis models for each slope zone were built based on GeoStudio software.

(1) Geometric model construction Slope geometric models were established in the SLOPE/W module using topographic lines, bench layout and geological cross-sections provided by the mine. The model scope fully considers the propagation path of potential slip surfaces: the model extends 50 m backward beyond the potential tension crack zone at the slope crest and 50 m forward below the potential shear outlet at the slope toe, eliminating boundary effects on automatic searching of critical slip surfaces.

(2) Material parameter assignment Each rock and soil stratum was generalized as homogeneous material, and the Mohr-Coulomb strength criterion was adopted.

(3) Boundary condition setup ① Displacement boundary: the model bottom is fixed to restrict horizontal and vertical displacement; rolling supports are set on both sides to limit horizontal displacement and allow vertical displacement. ② Hydraulic boundary: slope surfaces are free overflow boundaries; the model bottom is impermeable; both lateral sides are assigned constant head or flux boundaries according to actual hydrogeological conditions. ③ Load boundary: slope surfaces are free boundaries; seismic loads are applied under load combination II and load combination III.

(4) Simulation of freeze-thaw effects The mining area is located on a plateau subject to freeze-thaw cycles driven by snow and ice. Massive snowmelt water infiltrates slope surface rock masses with highly weathered and densely developed joints, saturating shallow rock masses and deteriorating their mechanical properties, which further reduces

overall slope stability. Therefore, the rock and soil within the upper 40m of slope surface were set to saturated state for numerical simulation.

4.3 Groundwater Seepage Field

Groundwater seepage significantly influences slope stability: pore water pressure forms in pores and fractures, generating static and hydrodynamic pressure on rock masses. Static buoyant pressure reduces effective normal stress on slip surfaces and weakens anti-sliding resistance; hydrodynamic seepage force increases the sliding force of slope masses. Both effects deteriorate slope stability. Thus, seepage field simulation is indispensable for any slope containing groundwater.

The stability of open-pit slopes is highly sensitive to groundwater distribution. The Seep/W finite element seepage module of GeoStudio software was utilized to simulate saturated-unsaturated seepage of typical slope profiles, identify the location and morphology of phreatic lines, and reveal the distribution law of pore water pressure inside slopes. The steady-state pore water pressure field calculated from seepage simulation was imported into SLOPE/W for fluid-solid coupling stability calculation to improve evaluation accuracy.

Boundary conditions were defined based on hydrogeological data and groundwater monitoring data of the mining area: (1) Upstream boundary: constant hydraulic head boundary was assigned at the far end of the model, with total head determined by the groundwater elevation at that location. (2) Downstream boundary: potential overflow boundaries were set at the pit bottom and slope toe to simulate free groundwater discharge and water convergence toward the open pit. (3) Bottom and lateral boundaries: defined as impermeable boundaries.

Seepage calculation was conducted using measured rock mass permeability coefficients and groundwater levels to obtain phreatic lines and pore water pressure distribution within slopes. The seepage simulation results of typical slope profiles are shown in Figure 4.

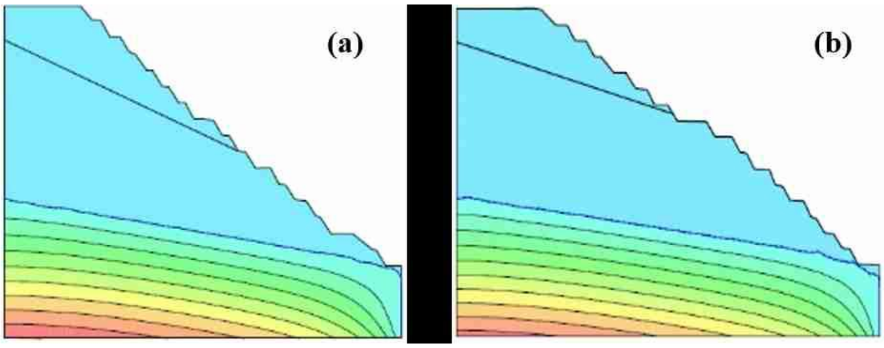

Figure 4 Seepage Field Simulation Results of Typical Slope Profiles: (a) Profile JX-N-1; (b) Profile JX-N-2

The simulation reproduced the current phreatic line distribution inside slopes. In practice, the groundwater level declines gradually with progressive open-pit excavation, which is beneficial to slope stability. Seepage analysis results indicate that the pore water pressure distribution conforms to hydrostatic rules: positive pore water pressure exists below the phreatic line and increases with depth; negative pore water pressure appears in the unsaturated zone above the phreatic line. The phreatic surfaces of all slopes are generally flat and positioned at low elevation, resulting in relatively weak static and hydrodynamic pressure.

4.4 Slope Stability Analysis under Different Load Combinations

Load combinations only consider slope self-weight and groundwater effects. GeoStudio software was adopted to calculate the overall stability of slopes. The Sarma method and Spencer method were used to compute safety factors of polygonal slip surfaces for slopes in the Jingxi-Barak mining area. For Profile JX-N-1, the safety factor calculated by both Sarma and Spencer methods equals 2.077, as shown in Figure 5.

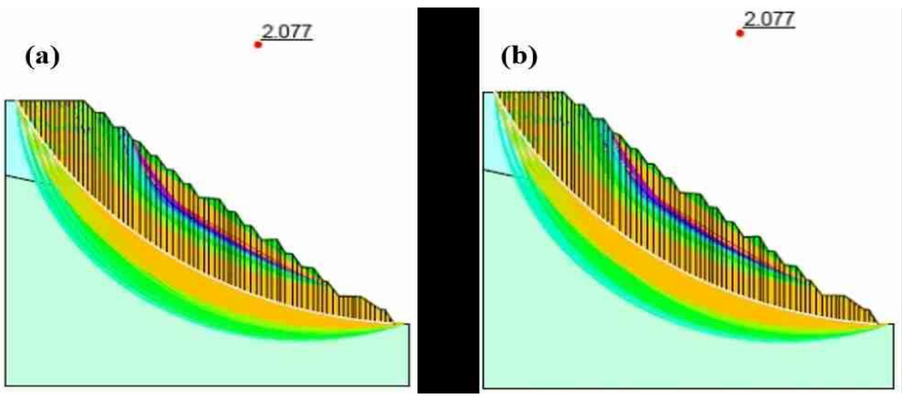

Figure 5 Stability Calculation Results of Profile JX-N-1 under Load Combination: (a) Sarma method,-2.077; (b) Spencer method,-2.077

For Profile JX-N-2, the safety factors calculated by the Sarma method and Spencer method are 2.246 and 2.247 respectively, as shown in Figure 6.

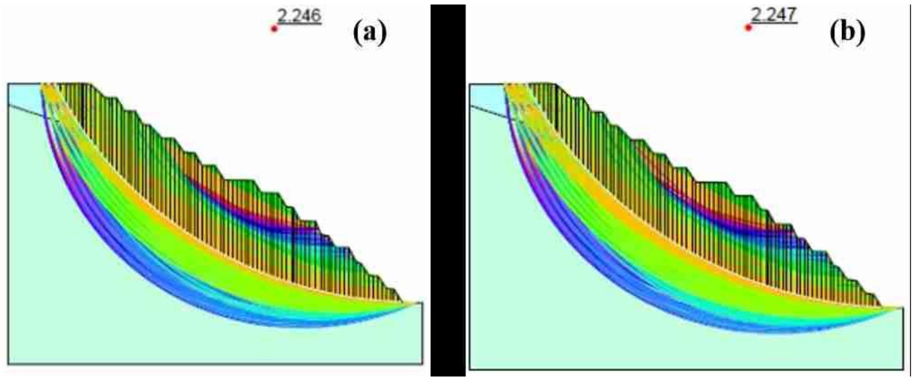

Figure 6 Stability Calculation Results of Profile JX-N-2 under Load Combination: (a) Sarma method,-2.246; (b) Spencer method,-2.247

In summary, the safety factors of slopes in the Jingxi-Barak mining area under the studied load combination range from 2.077 to 2.247, all exceeding the allowable safety factor of 1.25 specified in relevant codes, which proves that the overall slopes are in a stable state.

5 CONCLUSIONS

(1) Field sampling, specimen processing and indoor physical and mechanical tests were carried out to obtain comprehensive physical and mechanical parameters of tuff, limestone, tuffaceous sandstone and crystal tuff under natural and saturated conditions, including density, P-wave velocity, uniaxial compressive strength, tensile strength, cohesion and internal friction angle. The test data provide fundamental support for rock mass quality evaluation and slope stability analysis of the mining area.

(2) Numerical models of typical slope profiles were established via GeoStudio software. Limit equilibrium analysis using the Sarma method and Spencer method was performed for slopes in the Jingxi-Barak mining area. The safety factors of slopes under the studied load combination range from 2.077 to 2.247, all higher than the allowable safety factor of 1.25, demonstrating the overall stable state of open-pit slopes in the mining area.

COMPETING INTERESTS

The authors have no relevant financial or non-financial interests to disclose.

REFERENCES

[1] Zheng Y R, Zhao S Y, Shi W M, et al. Advances in slope stability analysis. Underground Space, 2001, 21(4): 262-271.
[2] Gu D Z. Fundamentals of Rock Mass Engineering Geomechanics. Beijing: Science Press, 1979.
[3] Sun Y K, Gu X. Application of Stereographic Projection in Rock Mass Engineering Geomechanics. Beijing: Science Press, 1980.
[4] Wang S J. Stereographic Projection and Its Application in Rock Mass Engineering. Beijing: Science Press, 1976.
[5] Fan G, Zhang J J, Fu X. Difference in dynamic response of bedding and anti-dip rock slopes containing mud interlayers. Chinese Journal of Geotechnical Engineering, 2015, 37(4): 692-699.
[6] Goodman R E, Kieffer D S. Behavior of Rock in Slopes. Journal of Geotechnical and Geoenvironmental Engineering, 2000, 126(8): 675-684.
[7] Li Z, Wang J X. Lower bound finite element plastic limit analysis of rock slopes based on nonlinear programming. Chinese Journal of Rock Mechanics and Engineering, 2007, 26(4): 747-753.
[8] Zuo B C, Chen C X, Liu X W, et al. Model test study on failure mechanism of anti-dip rock slopes. Chinese Journal of Rock Mechanics and Engineering, 2005, 24(19): 3505-3511.
[9] Ding X L, Fu J, Liu J, et al. Creep characteristics and stability analysis of slopes with interbedded soft and hard rock layers. Chinese Journal of Rock Mechanics and Engineering, 2005, 24(19): 3410-3418.
[10] Guo Z, Liu X P, Huang G P. Numerical simulation and dynamic response analysis of rock slope stability. Highway Engineering, 2012(5): 23-28.
[11] Huang Q X, Wang J L. Deformation characteristics of an anti-dip rock slope with weak interlayers. China Civil Engineering Journal, 2011, 44(5): 109-114.

APPENDIX

Table S1 Summary of Laboratory Physical and Mechanical Test Results of Rock Samples

	Density experiment	Wave velocity experiment	Uniaxial compression experiment				Splitting tensile test	Variable angle modulus shear experiment		Remark
lithology	Dry density (g/cm^3)	Longitudinal wave velocity V_p (m/s)	Uniaxial compressive strength σ_c/σ_w (MPa)	Modulus of elasticity (MPa)	Poisson's ratio μ	softening coefficient R	compressive strength σ_c (MPa)	Cohesion C (MPa)	internal friction φ (°)	Handling Status
Tuff	2.69	6.10	96.72	63.79	0.26	0.93	6.21	39.20	35.6	Dry
	2.73	6.77	93.76	61.40	0.35		8.22	34.03	35.78	Saturation
Limestone	2.66	6.31	82.71	66.71	0.29	0.88	6.88	16.86	36.66	Dry
	2.69	6.76	76.70	61.79	0.31		7.65	12.95	33.20	Saturation
Tuffaceous	2.66	5.71	78.67	74.41	0.35	0.79	7.92	27.14	39.21	Dry
sandstone	2.68	5.78	71.39	66.93	0.37		8.83	20.99	41.70	Saturation
Crystal	2.50	4.71	74.51	60.69	0.29	0.40	8.62	38.62	40.97	Dry
tuff	2.53	4.73	25.56	45.91	0.31		10.25	30.02	41.30	Saturation